

Charge-orbital ordering in low-temperature structures of magnetite: GGA+*U* investigationsHorng-Tay Jeng,^{1,2,*} G. Y. Guo,^{3,4,†} and D. J. Huang^{4,2}¹*Institute of Physics, Academia Sinica, Taipei 11529, Taiwan*²*Department of Physics, National Tsing Hua University, Hsinchu 300, Taiwan*³*Department of Physics, National Taiwan University, Taipei 106, Taiwan*⁴*National Synchrotron Radiation Research Center, Hsinchu 30076, Taiwan*

(Received 22 June 2006; revised manuscript received 21 September 2006; published 20 November 2006)

The atomic and electronic structure of magnetite (Fe_3O_4) in the four possible low-temperature structures, namely, $P2_1/c-Pmca$ (I), $Pmca$ (II), $Pmc2_1$ (III), and Cc (IV), have been investigated by generalized gradient approximation+Hubbard U (GGA+ U) electronic structure and structural optimization calculations. Charge-orbital ordering is found to exist in all the four structures. The charge-orbital ordering and hence the Verwey metal-insulator transition is shown to be driven by the on-site Fe d -electron correlation. The theoretical charge-orbital ordering patterns in the I, II, and III structures do not satisfy the Anderson criterion but are consistent with recent neutron and x-ray diffraction experiments. The IV (Cc) structure is found to be the ground state structure. In the IV structure, the charge-orbital ordering on 3/4 of the tetrahedra does not satisfy the Anderson condition, while on 1/4 of the tetrahedra it does. The observed entropy change at the Verwey transition, which has been a long standing puzzle, is analyzed and found to be consistent with the charge-orbital orders obtained here.

DOI: [10.1103/PhysRevB.74.195115](https://doi.org/10.1103/PhysRevB.74.195115)

PACS number(s): 71.20.-b, 31.15.Ar, 32.10.Dk

I. INTRODUCTION

Many transition-metal oxides¹⁻⁵ exhibit charge and orbital orderings, which manifest themselves in the spatial localization of the charge carriers on certain ionic sites and in the real space ordering of the charge carriers in particular electron orbitals, respectively. The physical properties, such as electric transport and magnetism, of transition-metal oxides are intimately related to charge and orbital orderings. Therefore, the fundamental mechanisms that give rise to charge and orbital orderings are of considerable current interest.⁶⁻⁹ However, the classic charge ordering problem is the metal-insulator transition in magnetite (Fe_3O_4),¹⁰ known as the Verwey transition, which has intrigued generations of solid-state physicists. Despite intensive theoretical and experimental investigations in the past 60 years, the origin and mechanism of the Verwey transition¹⁰ remains to be a matter of debate.¹¹

Magnetite is a mixed-valence $3d$ transition-metal oxide with formal chemical formula $\text{Fe}_A^{3+}[\text{Fe}^{2+}\text{Fe}^{3+}]_B\text{O}_4^{2-}$. At room temperature (T), it crystallizes in the inverse cubic spinel structure ($Fd\bar{3}m$) with two chemical formulas per unit cell. The oxygen ions form eight interpenetrating face-centered-cubic (fcc) lattices with the iron ions occupying the interstitial sites. One third of the Fe ions (Fe^{3+}) occupy the tetrahedral A -sites which form a diamond structure, while the remaining Fe ions with equal numbers of Fe^{2+} and Fe^{3+} ions, are located on the octahedral B -sites which form a corner-sharing tetrahedra network, as illustrated in Fig. 1. It is a metal with a moderate electric conductivity. However, on cooling below ~ 120 K, the Verwey temperature (T_V), Fe_3O_4 undergoes a first-order phase transition, in which the electrical conductivity abruptly decreases by two orders of magnitude.¹⁰ Assuming the high- T metallic conductivity is due to fast electron hopping between the B -site Fe^{2+} and Fe^{3+} ions, Verwey *et al.*¹⁰ interpreted this metal-insulator transition as a charge ordering of the Fe^{2+} and Fe^{3+} states on the

B -sites in successive (001) planes (Fig. 1), resulting in an orthorhombic structure (Verwey charge ordering model). Nevertheless, this appealing Verwey model was disproved by later experiments¹¹ which showed that low- T structure of magnetite is monoclinic rather than orthorhombic.

Magnetite became the subject of intensive theoretical and experimental studies in the following decades.¹¹ In particular, Anderson¹² studied the charge ordering on the corner-sharing B -site Fe tetrahedron network (Fig. 1) in magnetite and pointed out that each B -site Fe tetrahedron should contain two Fe^{2+} and two Fe^{3+} ions in order to minimize the electrostatic energy. This is known as the Anderson criterion and has been used to screen many charge ordering models proposed for magnetite.¹³⁻¹⁵ The Verwey model of charge ordering does satisfy the Anderson condition.¹² However, despite intensive investigations in the past 60 years, the detailed pattern or even the existence of the charge ordering in magnetite, or in general the crystal structure below the Verwey transition, is still not fully resolved.¹¹

Recently, Wright *et al.*^{16,17} found evidence of the long range charge ordering state with ionicity of +2.4 and +2.6 over B -site Fe ions using high-resolution neutron and synchrotron x-ray powder-diffraction data. Interestingly, the observed charge ordering^{16,17} is much more complicated than the Verwey model,¹⁰ and, especially, does not meet the seminal Anderson condition.¹² This has stimulated intensive renewed theoretical and experimental interest in recent years.¹⁸⁻²⁵ In particular, our generalized gradient approximation+Hubbard U (GGA+ U) calculations¹⁹ and also that of Leonov *et al.*,²⁰ using the refined low- T monoclinic $P2_1/c$ structure,¹⁷ not only corroborate the observed charge-ordering in Fe_3O_4 , but also reveal an associated t_{2g} orbital ordering on the B -site Fe sublattices. This discovered Fe t_{2g} orbital ordering¹⁹ offers an explanation for why the Anderson condition is not met by the observed charge ordering^{16,17} However, the work of Wright *et al.*^{16,17} was

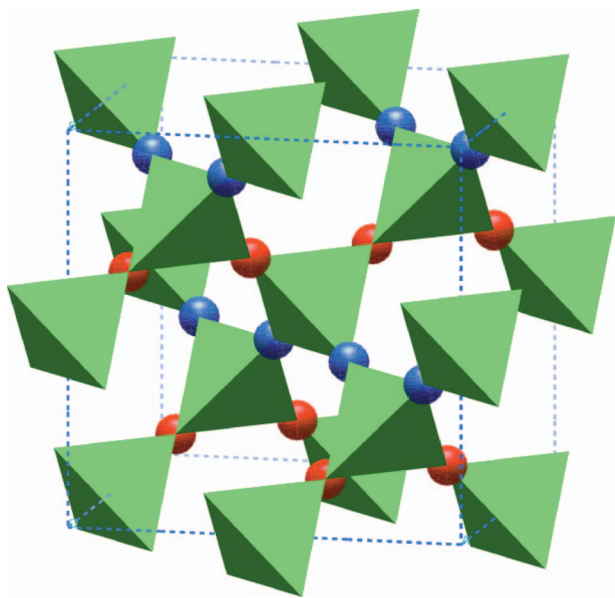


FIG. 1. (Color) Verwey charge ordering in the corner-sharing B -site Fe tetrahedron (green) network of Fe_3O_4 . The red and blue balls denote divalent and trivalent $\text{Fe}(B)$ ions, respectively. The A -site Fe and O ions are not shown here for simplicity. A complete crystal structure of high-temperature Fe_3O_4 can be found in, for example, Ref. 37.

challenged by a recent resonant Fe K -edge x-ray scattering investigation²¹ which was concluded that there is no charge ordering in magnetite. Furthermore, based on their high pressure x-ray powder diffraction measurements, Rozenberg *et al.*,²² very recently proposed that the Verwey transition is just an ordinary structural transition, perhaps driven by phonon-driven charge density wave. Nonetheless, much earlier neutron scattering measurements on phonon band structure of magnetite²⁶ already showed no evidence for any phonon softening. Amusingly, very recent O K -edge resonant x-ray scattering measurements²³ reveal clear experimental evidence for the existence of charge-orbital ordering in magnetite along the c -axis below the Verwey transition, being consistent with the GGA+ U calculations.¹⁹ More dramatically, evidence for the charge-orbital ordering on the B -site Fe sublattices have been found in the latest soft x-ray Fe $L_{2,3}$ resonant diffraction experiments.²⁴

In the last two decades, though the symmetry of the low- T structure of Fe_3O_4 have been known to be the monoclinic Cc symmetry^{13,16,17,27} with a sophisticated unit cell of 224 atoms, the detailed low- T atomic positions and ionic arrangement remains to be an open question.^{13–17,28} In the recent work by Wright and co-workers,^{16,17} a subcell of the Cc structure in the $P2/c$ symmetry was used for the atomic coordinates refinement with additional $Pmca$ (Refs. 17 and 27) or $Pmc2_1$ (Ref. 27) orthorhombic symmetry constraints in order to reduce the complexity. In the recent GGA+ U calculations,¹⁹ this reduced structure was used. Consequently, several questions remain to be answered. In particular, does the charge-orbital ordering also exist in the other proposed low- T structures? If it does, what is the driving force? Do the theoretically determined atomic coordinates and lattice parameters agree with that inferred from diffrac-

tion and scattering experiments? What structure among the proposed low- T structures is the ground state structure? In this paper, we present extensive electronic structure calculations including the total energy, U -dependence, structural optimization, charge-orbital ordering, for all the four proposed low- T structures in order to address the above-mentioned questions.

Another fundamental issue concerning the Verwey transition in magnetite is the observed entropy change at the Verwey transition. The expected entropy change of $2R \ln 2$ per mole from a complete charge order-disorder transition on the B -site Fe lattice, is nearly two times larger than the observed entropy change of $\sim R \ln 2$ per mole (where R is the gas constant).^{29,30} Anderson pointed out the essential role of short-range order (SRO) in the thermodynamics of the Verwey transition. Under the Anderson condition, the entropy problem in low- T magnetite is analogous to the old problem of the zero-point entropy of ice.¹² Assuming the SRO above the Verwey transition, the entropy change at the transition is derived to be $R \ln(3/2)$ per mole,¹² which is, however, $\sim 40\%$ smaller than $R \ln 2$ per mole observed in heat capacity measurement.^{29,30} Therefore, another purpose of the present paper is to address this interesting issue by using the calculated charge-orbital ordering pattern in magnetite.

The rest of the paper is organized as follows. The computational details are described in the next section. In Sec. III, we first summarize the calculated electronic structure of the $P2/c$ structure. In Sec. IV, we study the U dependence of the electronic structure of both the ideal cubic and $P2/c$ structures and demonstrate explicitly that the on-site Coulomb correlation is the driving force for the charge-orbital ordering and hence the Verwey transition. This is followed by a report on the results of the structural optimization calculations in Sec. V. In Sec. VI, the calculated charge-orbital ordering pattern in the Cc structure is presented. In Sec. VII, we address the anomalous entropy change at the Verwey transition in terms of the various theoretically found charge-orbital ordering patterns. Finally, the conclusions from this work are given in Sec. VIII.

II. COMPUTATIONAL DETAILS

Band structure calculations for the four possible low- T structures of magnetite, namely, $P2/c-Pmca$ (Ref. 17) (I), $Pmca$ (Ref. 27) (II), $Pmc2_1$ (Ref. 27) (III), and Cc (Ref. 13) (IV), were performed using the accurate frozen-core full-potential projector augmented wave method,³¹ as implemented in the VASP package.³² The calculations are based on the generalized gradient approximation (GGA) (Ref. 33) plus on-site Coulomb interaction U (GGA+ U) (Refs. 34 and 35) scheme. For the I, II, and III structures with 8 formula unit (f.u.) (56 atoms) in the $a_c/\sqrt{2} \times a_c/\sqrt{2} \times 2a_c$ (a_c is the cubic cell parameter) unit cell, the calculations were performed over a $6 \times 6 \times 2$ Monkhorst-Pack k -point grid in the Brillouin zone, while a $3 \times 3 \times 3$ k -point mesh was used for the IV structure with 32 f.u. (224 atoms) in the complex $\sqrt{2}a_c \times \sqrt{2}a_c \times 2a_c$ Cc supercell. To ensure the calculations be sufficiently accurate, 75 600 plane waves for the I, II, and III

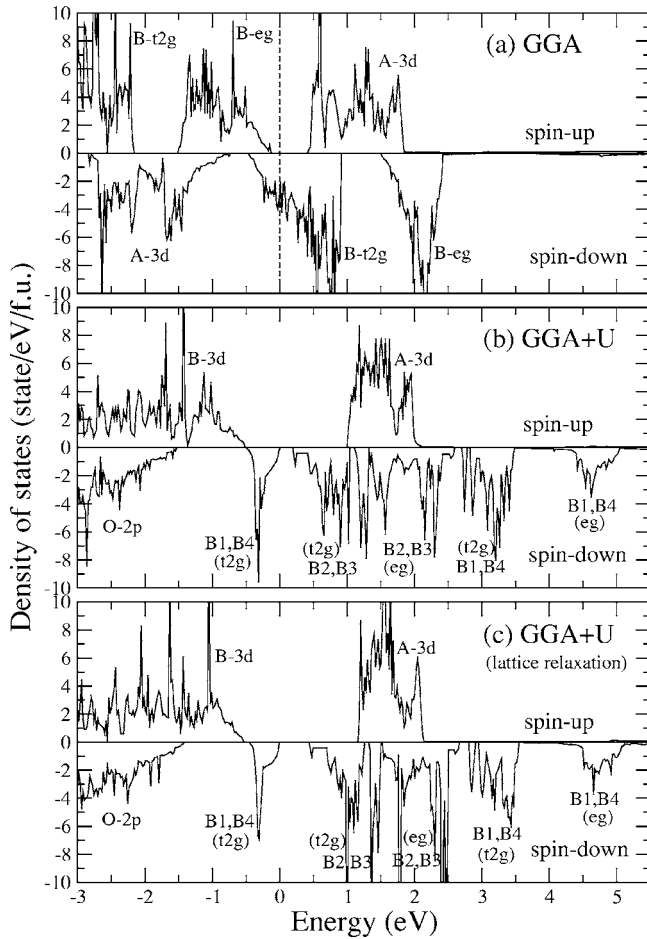


FIG. 2. Spin-resolved density of states of Fe_3O_4 in low- T monoclinic $P2/c$ structure from GGA (a), GGA+ U (b), and GGA+ U under lattice relaxation (c). The Fermi level is at zero energy.

structures, and 302 400 plane waves for the IV structure with the same cutoff energy of 400 eV, was used. On-site Coulomb energy $U=4.5$ eV (Ref. 36) and exchange parameter $J=0.89$ eV (Ref. 34) were used for all the Fe ions throughout except stated otherwise. In the structure optimization calculations, the experimental lattice parameters and atomic positions of the four low- T structures were used as inputs, and both the lattice constants and atomic positions are fully relaxed. The structure optimization processes stop when the total energy change falls below the small threshold of 0.001 eV/cell. The corresponding atomic forces and cell stresses of the optimized lattice structures all fall below 0.01 eV/Å and 1.0 kBar, respectively.

III. ELECTRONIC STRUCTURE OF THE $P2/c$ STRUCTURE

To set the stage for discussion, we first summarize the results of our GGA+ U calculations for the experimentally determined low- T monoclinic $P2/c$ (I) structure¹⁷ of magnetite reported in Ref. 19. The GGA calculations predict that the low- T phase [Fig. 2(a)] is a half-metallic ferrimagnet in which there is a gap at the Fermi level in the spin-up channel while the band structure for the spin-down channel is metal-

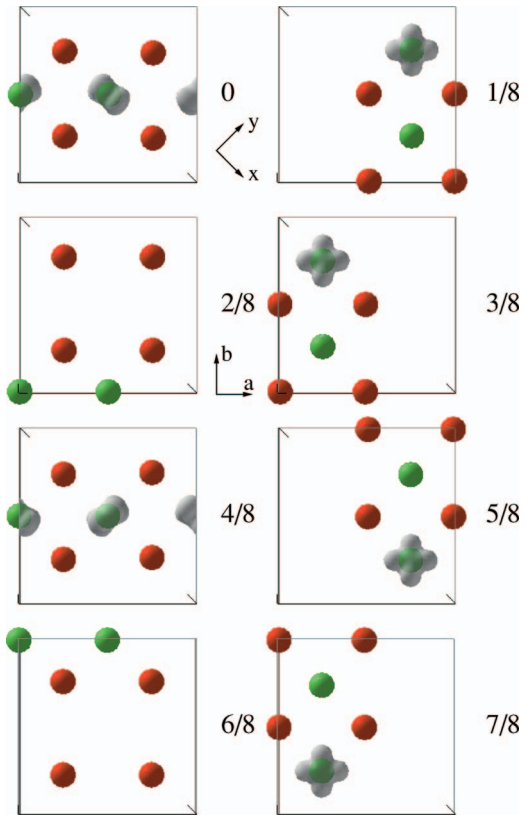


FIG. 3. (Color) Charge-orbital ordering on B -site sublattice in $P2/c$ Fe_3O_4 . The green and red balls denote $\text{Fe}(B)$ and O ions, respectively. Isocharge surface (gray) indicates d_{yz} , d_{xz} , and d_{xy} orbitals on $\text{Fe}(B)$ ions. a - b and x - y are global and local coordinates, respectively.

lic, being similar to the previous LDA calculations for Fe_3O_4 in the high- T cubic phase.³⁷ The conduction band in the spin down channel near the Fermi level is predominantly of $\text{Fe}(B)$ - t_{2g} character. However, when the on-site Coulomb energy $U=4.5$ eV, which eliminates the spurious self-interaction and relatively localizes 3d orbitals, is taken into account, the half-metallic band structure in the low- T phase becomes an insulating one [Fig. 2(b)]. As a result, an energy gap of 0.2 eV is opened in the spin-down $\text{Fe}(B)$ - t_{2g} band at the Fermi level, being consistent with the experimental gap of 0.14 eV from measurements of the optical-conductivity spectrum.³⁸

The lattice distortion in the low- T phase lowers the site symmetry and the B -site Fe ions break into six inequivalent types, namely, $\text{Fe}(B1a)$, $\text{Fe}(B1b)$, $\text{Fe}(B2a)$, $\text{Fe}(B2b)$, $\text{Fe}(B3)$, and $\text{Fe}(B4)$. As indicated in Fig. 2(b), the occupied spin-down t_{2g} band belongs to the charge-rich $\text{Fe}(B1)$ and $\text{Fe}(B4)$ ions, suggesting the existence of charge ordering. The calculated valence charge density distribution and orbital-decomposed densities of states¹⁹ clearly show the formation of an orbital ordering on the divalent B -site sublattice in which one extra conduction electron occupies the spin-down d_{yz} , d_{xz} , and d_{xy} orbitals of $\text{Fe}(B1a)$, $\text{Fe}(B1b)$, and $\text{Fe}(B4)$, respectively. In this orbital ordered state, the spin-down t_{2g} electron cloud of the three divalent $\text{Fe}(B)$ ions arrange themselves with one lobe of each electron cloud pointing towards

TABLE I. Calculated properties of Fe_3O_4 in monoclinic $P2/c$ and ideal cubic phase from GGA and GGA+ U using $a_c/\sqrt{2} \times a_c/\sqrt{2} \times 2a_c$ unit cell. Charge separations (CS) were calculated within atomic spheres of radius 1.0 Å. OO represents orbital ordering (the orbital-order parameter P is given in the parentheses). Total energy (E_t) is relative to the total energy of the ideal cubic primitive cell (internal parameter $u=0.0$) with the corresponding U and J values.

$P2/c$					Cubic supercell $a_c/\sqrt{2} \times a_c/\sqrt{2} \times 2a_c$			
U eV	\downarrow gap eV	CS e	OO(P)	E_t eV/f.u.	\downarrow gap	CS e	OO(P)	E_t eV/f.u.
0.0	No	0.00	No(0.55)	-0.15	No	0.00	No(0.34)	0.00
4.0	No	0.11	Yes(0.98)	-0.53	No	0.10	Yes(0.96)	-0.22
4.5	0.20	0.15	Yes(0.98)	-0.62	No	0.12	Yes(0.96)	-0.27
5.0	0.42	0.17	Yes(0.97)	-0.72	0.11	0.16	Yes(0.96)	-0.35
5.5	0.63	0.19	Yes(0.96)	-0.85	0.28	0.19	Yes(0.91)	-0.47

the trivalent Fe($B3$) ion due to the intersite Coulomb attraction energies between the trivalent Fe($B3$) and the down-spin electron clouds of divalent Fe($B1a$), Fe($B1b$), and Fe($B4$) ions. Such intersite Coulomb attractions cause one of the most significant atomic position deformations at the Verwey transition that the Fe($B3$) ion on one of the vertices of the Fe(B)-O cube is strongly pulled inwards along the cube diagonal. The charge-orbital ordering results mainly from the on-site U , as will be demonstrated by explicit GGA+ U calculations with different values of U below. The formation of the orbital order subsequently induces the structural distortion which re-enforce the charge-orbital order. To see clearly the charge-orbital ordering pattern along c direction, we present in Fig. 3 the charge-density contours corresponding to the energy interval between the Fermi level (0) and 0.5 eV below it (-0.5 eV). It can be seen clearly from Fig. 3 that the charge-orbital ordering can be considered as the superposition of $[001]_c$ and $[00\frac{1}{2}]_c$ charge density wave modulations, as pointed out by Wright *et al.*¹⁶

IV. IMPORTANCE OF THE ON-SITE COULOMB INTERACTION U

To unravel the origin of the formation of the charge-orbital ordered state and subsequently opening of the insulating energy gap at the Fermi level in magnetite below the Verwey temperature, let us examine the effects of on-site U and lattice distortion on the electronic structure. In Table I, we list the calculated properties of magnetite in both the monoclinic $P2/c$ structure and the ideal cubic structure with a $a_c/\sqrt{2} \times a_c/\sqrt{2} \times 2a_c$ supercell corresponding to high- T fcc lattice with internal parameter $u=0.0$, from the GGA ($U=0.0$ eV) and GGA+ U calculations with different U values. The spin-down energy gap at the Fermi level, the charge separations between the charge-rich and charge-poor Fe(B) in the charge ordering state, and the existence of orbital ordering are listed in the three columns of both the $P2/c$ and cubic blocks, respectively. To indicate the amplitude of orbital order, we use a simple parameter P to represent the

distribution of the orbital occupancy among the three spin-down t_{2g} orbitals of the Fe($B1a$) ion, namely, $P = n(d_{yz})/n(t_{2g})$ where n is the occupation number. In this definition, the orbital order parameter would be 1/3 (evenly distributed among the three t_{2g} orbitals) in the cases without orbital order, whereas it would be 1.0 in the perfectly orbital ordered cases. In the pure GGA case ($U=0.0$), the gap, charge-ordering (CO), and orbital ordering (OO) are all absent whether the lattice distortion is taken into account or not. The orbital-order parameter is approximately 1/3 (Table I) in the ideal cubic structure without orbital ordering, while in the real $P2/c$ lattice, the orbital-order parameter is about 1/2 (Table I), indicating that there exists slight orbital polarization due to the lattice distortion. However this slight orbital polarization is far shorter than those of the orbital-ordered cases ($P>0.9$) as discussed below. In the $U=4.5$ eV case, the $P2/c$ structure exhibits a charge-orbital ordered state ($P=0.98$) with an insulating band gap of 0.20 eV and a charge separation of 0.15 e . Furthermore, even in the ideal cubic supercell structure in which the lattice distortion is not present, the OO ($P=0.96$) similar to that in the $P2/c$ case, persists, though the charge separation is reduced to 0.12 e and the small insulating gap is closed. For a smaller U value of 4.0 eV, in the $P2/c$ structure, the energy gap is also eliminated and the charge separation is reduced to 0.11 e while the OO still exists. These results imply that near $U=4.5$ eV, the effect of the lattice distortion is roughly equivalent to that from increasing the U value by about 0.5 eV. For larger U values of, e.g., 5.0 and 5.5 eV, the energy gaps and charge separations are enhanced in both the $P2/c$ and cubic structures. Interestingly, as shown in Table I, with $U \geq 5.0$ eV, even the undistorted cubic structure exhibits a charge-orbital ordered state with an insulating energy gap of 0.11 eV. Therefore, we may conclude that, rather than being an ordinary structural phase transition,²² the Verwey metal-insulator transition is an on-site electron correlation-driven charge-orbital ordering, which results in the corresponding lattice distortion and the subsequent opening of the insulating gap.¹⁹

The reason why the charge ordering has been so difficult to observe despite of intensive experimental effort in the past

TABLE II. Calculated properties of Fe_3O_4 in low- T structures I [$P2/c$ - $Pmca$ (Ref. 17)], II [$Pmca$ (Ref. 27)], III [$Pmc2_1$ (Ref. 27)], and IV [Cc (Ref. 13)] from GGA+ U with $U=4.5$ eV. The lower panel contains the corresponding results from the fully relaxed lattices. Charge separations (CS) were calculated within atomic spheres of radius 1.0 Å. OO represents orbital ordering (the orbital-order parameter P is given in the parentheses). Total energy (E_t) is relative to the total energy of the experimental cubic primitive cell (internal parameter $u=0.005$) with the corresponding U and J values.

Fe_3O_4 lattice	↓gap (eV)	CS (e)	OO(P)	$\langle\text{Fe}_B^{2+}\text{-O}\rangle$ (Å)	$\langle\text{Fe}_B^{3+}\text{-O}\rangle$ (Å)	E_t (eV/f.u.)
I	0.20	0.15	Yes(0.98)	2.07	2.05	-0.3499
II	0.12	0.14	Yes(0.98)	2.07	2.05	-0.3281
III	No	0.12	Yes(0.97)	2.07	2.05	-0.2446
IV	0.20	0.13	Yes(0.96)	2.07	2.05	-0.2462
I.rlx	0.44	0.15	Yes(0.97)	2.09	2.03	-0.3822
II.rlx	0.44	0.15	Yes(0.97)	2.09	2.03	-0.3791
III.rlx	0.44	0.15	Yes(0.97)	2.09	2.03	-0.3787
IV.rlx	0.66	0.15	Yes(0.94)	2.09	2.03	-0.3957

decades, is clearly due to the smallness of the charge disproportionality because of the strong screening from 4s and 4p electrons. On the other hand, one should look for the orbital ordering, which is more fundamental and perhaps easier to probe, rather than the charge ordering. Encouragingly, latest O K -edge and also Fe $L_{2,3}$ -edge resonant x-ray scattering experiments^{23,24} provide solid evidence for the Fe(B) t_{2g} orbital ordering predicted in Ref. 19. The calculated total energies with respect to that of ideal $a_c/\sqrt{2} \times a_c/\sqrt{2} \times 2a_c$ lattice from different U values are listed in the last column of Table I. These results demonstrate that the formation of charge-orbital ordering (without lattice distortion) would lower the total energy by 0.22–0.47 eV/f.u. The significant energy gain indicates that the charge-orbital ordering induced by on-site U , plays an essential role in the Verwey transition. When the lattice distortion is also taken into account, the total energy would be further lowered by 0.53–0.85 eV/f.u.

V. EFFECT OF THE STRUCTURAL RELAXATIONS

In Table II, we list the calculated spin down energy gap at the Fermi level, charge separation, orbital ordering, averaged Fe(B)-O bond length, as well as the total energies (with respect to the total energy of the experimental high- T cubic lattice with internal parameter $u=0.005$) of the four known low- T Fe_3O_4 structures from the GGA+ U calculations with $U=4.5$ eV. The orbital-order parameter P of Fe($B1a$) in $P2/c$ structure mentioned in the preceding section as well as those of corresponding B -site Fe ions in the other three lattices are also given in the parentheses. For the experimental structures (upper block), the averaged bond length between the divalent-Fe(B) [trivalent-Fe(B)] ions and the neighboring oxygen ions are nearly the same, being about 2.07 Å (2.05 Å), though the obtained charge separations vary from 0.12 e to 0.15 e . There is some apparent correlation between the calculated charge separation and insulating gap. As shown in Table II, the III structure has the smallest charge separation of 0.12 e . As a result, the B -site spin-down t_{2g}

band splittings are significantly suppressed, and the insulating gap at the Fermi level in the spin-down channel disappears, as shown in Fig. 4(c). In contrast, the other three structures have an insulating gap ranging from 0.1 to 0.2 eV [Fig. 2(b) and Figs. 4(a) and 4(e)]. Furthermore, the total energy of structure III is about 0.1 eV/f.u. higher than both structures I and II with charge separations of 0.15 e and 0.14 e , respectively. However, the total energy of the III structure is only slightly (0.002 eV/f.u.) higher than structure IV which has a charge separation of 0.13 e .

The properties of fully relaxed low- T structures are also presented in the lower panel of Table II as well as in Fig. 2(c) and Figs. 4(b), 4(d), and 4(f). After the full lattice relaxation, the total energies of all the four structures become lowered and the total energy differences between the different structures are considerably reduced to within ± 0.01 eV/f.u. The most pronounced effect of the structural optimization is perhaps the relative stability of the four structures. After the full lattice relaxation, structure IV, i.e., the Cc structure with the cell size of $\sqrt{2}a_c \times \sqrt{2}a_c \times 2a_c$, has the lowest total energy, indicating that it is most likely to be the true low- T structure of magnetite. Nevertheless, as mentioned above, the total energy differences among the four structures are very small, and this perhaps explains why the four structures all have been observed experimentally. Another pronounced effect of the structural optimization is that the difference between the averaged bond lengths of $\langle\text{Fe}_B^{2+}\text{-O}\rangle$ and $\langle\text{Fe}_B^{3+}\text{-O}\rangle$ are increased from 0.02 Å to 0.06 Å. This enhanced bond length difference gives rise to an increased charge separation between the divalent and trivalent Fe(B), and hence a greater band splitting in spin-down Fe(B)- t_{2g} band. As shown in Table II, the spin down band gap is greatly enlarged to 0.44 eV for lattices I [Fig. 2(c)], II [Fig. 4(b)], and III [Fig. 4(d)], and to 0.66 eV for lattice IV [Fig. 4(f)] after the full lattice relaxation. The resultant energy gaps are somewhat larger than the band gap of 0.14 eV derived from optical-conductivity spectrum measurements,³⁸ suggesting that the on-site U of 4.5 eV (Ref. 35) used in the calculations could be slightly overestimated. Nevertheless, the conclusions

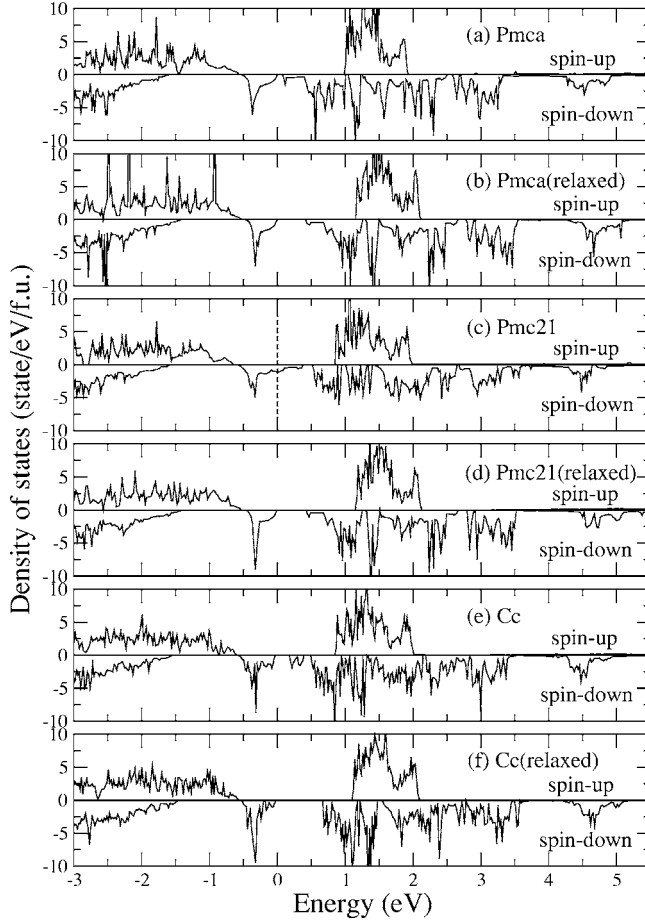


FIG. 4. Spin-resolved density of states of Fe_3O_4 in low- T $Pmca$ (a, b), $Pmc2_1$ (c, d), and Cc (e, f) lattices from GGA+ U and GGA+ U under lattice relaxation, respectively. The Fermi level is at zero energy.

emerged from the above discussion should remain unchanged. Interestingly, the full lattice relaxations result in the same charge separation of $0.15e$ for all the four structures. Finally, we note that the orbital ordering prevails in all the cases including the experimental and fully relaxed structures.

Theoretically refined lattice parameters and atomic positions of the low- T $P2/c$ and Cc structures are listed in Tables III and IV, respectively. Experimental data from Refs. 17 and 13 were used, respectively, as the initial inputs in the GGA+ U structure optimization calculations. The obtained $P2/c$ lattice parameters of $a=5.955$, $b=5.937$, and $c=16.710$ Å, and $\beta=90.237^\circ$ are very close to the corresponding experimental parameters of $a=5.944$, $b=5.925$, and $c=16.775$ Å, and $\beta=90.236^\circ$ (Ref. 17), respectively. The theoretical a and b parameters are slightly enhanced, whereas the theoretical c constant is slightly reduced, with the theoretical volume being $\sim 0.01\%$ smaller than the experimental one. After the lattice relaxation, in the $P2/c$ structure, the atomic coordinates (Table III) remain more or less the same as the experimental ones¹⁷ with the maximum deviation being $\sim 2\%$. For the Cc structure, the calculated lattice constants of $a=11.8838$, $b=11.8682$, and $c=16.7369$ Å, and $\beta=90.2006^\circ$ are also very close to the corresponding experimental values of $a=11.868$, $b=11.851$, and $c=16.752$ Å, and $\beta=90.20^\circ$,

TABLE III. Theoretical (GGA+ U) refined coordinates of magnetite in $P2/c$ symmetry with experimental data (Ref. 17) as initial inputs. The relaxed cell parameters are $a=5.9545$, $b=5.9372$, and $c=16.7098$ Å, and $\beta=90.2374^\circ$.

Atom	x	y	z
A(1)	0.2498	0.0099	0.0641
A(2)	0.2501	0.5051	0.1894
B(1a)	0.0000	0.5000	0.0000
B(1b)	0.5000	0.5000	0.0000
B(2b)	0.0000	0.0097	0.2500
B(2b)	0.5000	0.0097	0.2500
B(3)	0.2501	0.2648	0.3799
B(4)	0.2500	0.7534	0.3759
O(1)	0.2500	0.2653	0.9968
O(2)	0.2500	0.7554	0.9977
O(3)	0.2500	0.2410	0.2545
O(4)	0.2500	0.7750	0.2519
O(5a)	0.9923	0.0159	0.1304
O(5b)	0.4923	0.0160	0.3696
O(6b)	0.9920	0.4961	0.1268
O(6b)	0.4921	0.4961	0.3732

respectively. The slight change in the lattice shape is similar to that found in the $P2/c$ lattice. However, despite the good agreement (within $\sim 0.2\%$) between the experimental and theoretical Cc lattice volumes, the differences in the atomic positions can be rather significant. The calculated coordinates of some of the atoms (Table IV) can differ from the corresponding experimental coordinates (Table I of Ref. 13) by 3%–7%, indicating that these experimental atomic positions are unstable. Further analysis of the experimental data¹³ starting with the theoretical atomic positions may be useful. Such nontrivial atomic relaxations in the Cc lattice may significantly affect the charge-orbital ordering patterns, as discussed below.

VI. CHARGE-ORBITAL ORDERING IN THE Cc STRUCTURE

We notice that the charge-orbital ordering pattern is the same in both the unrelaxed and relaxed I, II, and III structures, as shown in Fig. 3. However, in contrast, the experimental Cc (IV) structure exhibits a different and complex charge-orbital ordering pattern. In Fig. 5, we display this spin-down charge-orbital ordering at various heights along the c axis in the unrelaxed Cc unit cell. It is clear from Fig. 5 that the charge-orbital ordering in the Cc cell at heights 0, $1/8$, $4/8$, and $5/8$ c is nearly identical to that in the smaller $P2/c$ cell (Fig. 3). Interestingly, compared with the charge-orbital ordering in the $P2/c$ structure (Fig. 3), half (two) of the occupied t_{2g} orbitals at heights $3/8$ and $7/8$ c disappear and the two electrons move to occupy two pairs of neighboring t_{2g} orbitals at $2/8$ and $6/8$ layers, respectively, forming a dimerlike orbital-ordering pattern (Fig. 5). Occupancy analysis reveals that the two B -site Fe ions forming each dimerlike

TABLE IV. Theoretical (GGA+ U) refined coordinates of magnetite in Cc symmetry with experimental data (Ref. 13) as initial inputs. The relaxed cell parameters are $a=11.8838$, $b=11.8682$, and $c=16.7369$ Å, and $\beta=90.2006^\circ$.

Atom	x	y	z	Atom	x	y	z
A(1)	0.2499	0.0055	0.0637	A(2)	0.2508	0.5052	0.0633
A(3)	0.2492	0.2503	0.1898	A(4)	0.2495	0.7543	0.1900
A(5)	0.0026	0.2542	0.3103	A(6)	0.9987	0.7521	0.3104
A(7)	0.9980	0.0033	0.4366	A(8)	0.0015	0.5034	0.4365
B(1)	0.1252	0.2506	0.0002	B(2)	0.3750	0.2507	0.0003
B(3)	0.6245	0.2512	0.0007	B(4)	0.8755	0.2510	0.0008
B(5)	0.9994	0.1326	0.1211	B(6)	0.0004	0.3768	0.1245
B(7)	0.0001	0.6329	0.1207	B(8)	0.9996	0.8765	0.1248
B(9)	0.1210	0.0043	0.2496	B(10)	0.3755	0.0043	0.2494
B(11)	0.6293	0.0058	0.2486	B(12)	0.8741	0.0051	0.2489
B(13)	0.2497	0.1269	0.3795	B(14)	0.2503	0.3774	0.3747
B(15)	0.2504	0.6356	0.3794	B(16)	0.2498	0.8762	0.3755
O(1)	0.0003	0.1233	0.0028	O(2)	0.0000	0.6230	0.0028
O(3)	0.9999	0.3686	0.0029	O(4)	0.9997	0.8681	0.0026
O(5)	0.1214	0.2480	0.1257	O(6)	0.3785	0.2479	0.1269
O(7)	0.1213	0.7482	0.1260	O(8)	0.3785	0.7484	0.1268
O(9)	0.1214	0.0078	0.1301	O(10)	0.1221	0.5082	0.1300
O(11)	0.3788	0.0081	0.1301	O(12)	0.3797	0.5082	0.1287
O(13)	0.0052	0.1251	0.2453	O(14)	0.9997	0.6199	0.2461
O(15)	0.9995	0.3881	0.2480	O(16)	0.0054	0.8828	0.2476
O(17)	0.2443	0.3819	0.2540	O(18)	0.2508	0.8884	0.2532
O(19)	0.2506	0.1190	0.2553	O(20)	0.2446	0.6260	0.2566
O(21)	0.1272	0.0087	0.3703	O(22)	0.3726	0.0087	0.3702
O(23)	0.1329	0.5016	0.3708	O(24)	0.3660	0.5015	0.3715
O(25)	0.1340	0.2533	0.3739	O(26)	0.3659	0.2536	0.3730
O(27)	0.1264	0.7473	0.3748	O(28)	0.3736	0.7475	0.3737
O(29)	0.2499	0.3672	0.4946	O(30)	0.2504	0.8672	0.4959
O(31)	0.2501	0.1217	0.4970	O(32)	0.2498	0.6222	0.4973

orbital order have $0.27e$ and $0.41e$, respectively, in their spin-down t_{2g} orbitals (Fig. 6, left-hand panel). Hence the total charge of $0.68e$ per dimer corresponds conceptually to one electron per bond. This appears to lend some support to the bond dimerization model proposed previously in Ref. 39 for the Verwey transition in magnetite, based on mean-field calculations and taking into account of the cooperative effects of strong electronic correlation and electron-phonon interaction. Note that the dimerlike charge-orbital ordering comes out naturally in the present unbiased GGA+ U calculations. However, the bond dimerization model proposed in Ref. 39 does not agree with the bond length analysis based on the experiments on magnetite in the $P2/c$ structure in Ref. 17. Furthermore, such a dimerlike charge-orbital ordering is actually unstable against structure optimization. After the structure optimization, one-half of the Fe(B)-O bond lengths of these dimers at $2/8$ and $6/8$ c are enhanced, and the other one-half are suppressed. As a result, the two t_{2g} electrons occupying two pairs of dimerlike orbitals (one electron per bond) in the unrelaxed Cc lattice concentrate themselves on two B -site Fe in the relaxed Cc lattice, leading

to an occupancy of $0.71e$ /divalent ion and of $0.07e$ /trivalent ion on the two B -site Fe ions, respectively, as shown on the right-hand panel of Fig. 6.

The charge-orbital ordering patterns at heights $2/8$, $3/8$, $6/8$, and $7/8$ in the theoretically optimized Cc cell are still different from those in the $P2/c$ cell as well as those in the experimental Cc cell. Importantly, the charge-orbital ordering in the theoretical Cc structure exhibits a distinct feature, namely, the majority ($3/4$) of the corner-sharing Fe(B) tetrahedra are composed of either three Fe^{2+} and one Fe^{3+} ions, or one Fe^{2+} and three Fe^{3+} ions (i.e., the so-called “3-1” charge ordering pattern), whereas the minority ($1/4$) consist of two Fe^{2+} and two Fe^{3+} ions (i.e., the so-called “2-2” charge ordering pattern). This is different from the purely “3-1” charge-orbital ordering pattern found in the $P2/c$ structure¹⁹ as well as in the II and III structures from the present calculations. Thus, in the Cc structure, the major part (the “3-1” pattern) of the charge-orbital ordering still does not satisfy Anderson’s “2-2” charge ordering criterion¹² that each corner-sharing B -site Fe tetrahedron must contain two Fe^{2+} and two Fe^{3+} ions to minimize the electrostatic energy,

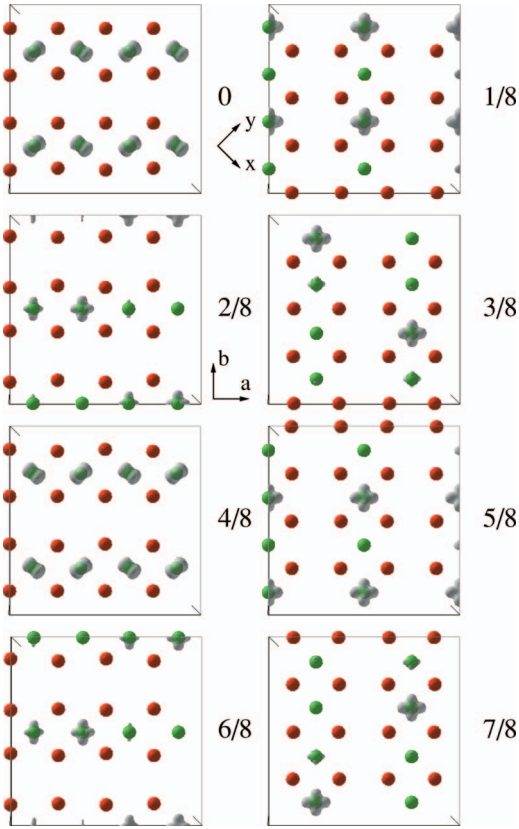


FIG. 5. (Color) Charge-orbital ordering on B -site sublattice in Cc Fe_3O_4 . The green and red balls denote $\text{Fe}(B)$ and O ions, respectively. Isocharge surface (gray) indicates d_{yz} , d_{xz} , and d_{xy} orbitals on $\text{Fe}(B)$ ions.

though the minor part (the “2-2” pattern) does. Moreover, as for the purely “3-1” charge-orbital ordering in the $P2/c$ structure,¹⁹ all the spin-down orbitals of the Fe^{2+} ions in the Cc lattice (Figs. 5 and 6) point one lobe of the electron cloud towards the neighboring Fe^{3+} ions so that the intersite Coulomb energy becomes lower. Clearly, further experiments such as resonant x-ray scattering measurements,²³ on magnetite in the low- T Cc structure are needed to determine the details of the actual charge-orbital ordering in Fe_3O_4 .

VII. ENTROPY CHANGE AT THE VERWEY TRANSITION

Another interesting issue is the entropy change at the Verwey transition. As mentioned in the Introduction, under the Anderson’s “2-2” charge-ordering condition, the entropy change from the fully ordered state below the Verwey transition to the complete disorder above it, would be $2R \ln 2$ per mole, being 2 times larger than $R \ln 2$ per mole observed in the heat capacity measurements.²⁹ One attempt to resolve this outstanding discrepancy has been to assume that at the temperatures immediately above the Verwey transition, magnetite exhibits the short range order rather than the complete disorder. For any “2-2” charge-ordering patterns, the entropy for the short range order is $R \ln(3/2)$ per mole.¹² Consequently, the associated entropy change would be $R \ln(3/2)$, which is, however, $\sim 40\%$

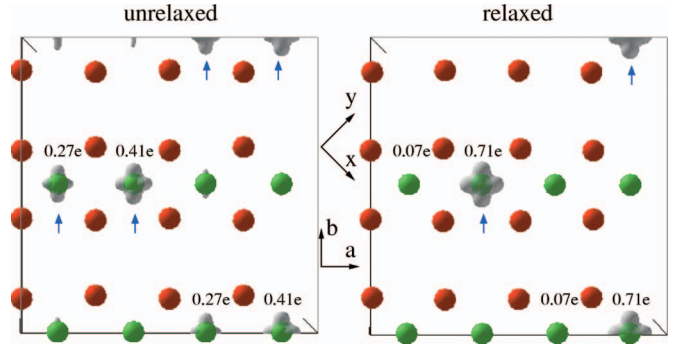


FIG. 6. (Color) Charge-orbital ordering on B -site sublattice at $2/8$ and $6/8$ c in experimentally observed (left-hand panel) and theoretically relaxed (right panel) lattice in Cc symmetry. The green and red balls denote $\text{Fe}(B)$ and O ions, respectively. The dimerlike (one electron per bond) charge distribution (indicated by blue arrows) in the unrelaxed lattice (left-hand panel) prefers to occupy a single site under lattice relaxation (right-hand panel). The occupation numbers are also given for the relevant ions.

smaller than the experimental value. Therefore, the observed entropy change at the Verwey transition, like Verwey transition itself, has been a puzzle despite intensive experimental and theoretical investigations in the past decades.²⁹

Following Anderson’s deduction¹² of entropy in magnetite under short range “2-2” order assumption over the two sets of tetrahedra (both contain $N/4$ tetrahedra, where N is the number of B -site Fe) with opposite orientations such that all those in one set touch only those in the other (Fig. 1), we find the entropy per mole for the short range “3-1” charge ordered state to be

$$S = k_B \ln W = R \ln 2,$$

where k_B is the Boltzmann constant and the number of total microstates

$$W = (1/2)^{N/4} (8)^{N/4} = (2)^{N/2}.$$

Therefore, the entropy change would be $R \ln 2$ per mole if the Verwey transition is assumed from the short range order above it to the long range order below it, being in excellent agreement with the experimentally observed value.²⁹ This clearly indicates that the “3-1” charge ordering found in both the experimental and theoretical optimized I, II, and III structures, not only is more realistic than the Anderson’s “2-2” charge ordering, but also helps to resolve the long standing puzzle of the entropy change at the Verwey transition. Furthermore, as mentioned in Sec. IV, the “3-1” charge-orbital ordering could also exist in the high- T undistorted cubic structure, and hence, it is likely that the short range order rather than the complete disorder, would appear at the temperatures above the Verwey transition. Indeed, indication of the existence of the short range order above the Verwey transition and below room temperature in diffuse neutron scattering,⁴⁰ optical conductivity experiments³⁸ and also some photoemission measurements,⁴¹ has been reported, though there is no evidence for the SRO in heat capacity experiments.^{29,30}

Nevertheless, as mentioned above, in the theoretically optimized IV structure, 3/4 of the Fe(B) tetrahedra exhibit the “3-1” charge ordering while the rest show the “2-2” charge ordering. The entropy associated with the short range order of this mixed charge ordering pattern is $R/4 \ln 12$ per mole. Therefore, the entropy change would be $R/4 \ln 12$ per mole if the Verwey transition is assumed to be from the short range order above it to the long range order below it. We note that this entropy change associated with the combined “3-1” and “2-2” charge ordering found in the theoretically optimized Cc (IV) structure is only $\sim 10\%$ smaller than the experimental value,²⁹ indicating the strong possibility of the existence of this mixed charge ordering pattern. Further experiments searching for the short range order above the Verwey transition are needed to finally clarify this long standing issue.

VIII. CONCLUSIONS

In conclusion, the atomic and electronic structures of magnetite in the four proposed low- T structures have been investigated in detail by using the GGA+ U method. All the four structures are found to exhibit a similar charge-orbital ordered state with charge separations of $0.12\text{--}0.15e$. Structures I, II, and IV are found to be an insulator with an energy gap of $0.1\text{--}0.2$ eV, whereas structure III is a half-metallic ferrimagnet. After lattice relaxation, all the four structures remain or become a charge-orbital ordered insulator with an

energy gap of $0.44\text{--}0.66$ eV, and with charge separations of $0.15e$. Lattice relaxation tends to eliminate the dimerlike orbital ordering found in unrelaxed lattice IV. The GGA+ U calculations also show that the IV (Cc) structure with the largest unit cell of 224 atoms is the most stable low- T structure. GGA+ U calculations further reveal that the IV structure has a mixed charge-orbital ordering pattern with 3/4 of the B -site tetrahedra showing the “3-1” charge-ordering pattern while 1/4 of the tetrahedra showing “2-2” ordering pattern. All the charge-orbital ordering patterns found in the low- T structures are found to be consistent with the observed entropy change at the Verwey transition if a short-range order rather than the completely disorder is assumed in the temperatures immediately above the Verwey transition. Finally, the on-site Coulomb repulsion U is explicitly shown to be the origin of the charge-orbital ordering, the associated lattice distortion, and hence the Verwey metal-insulator transition. Hopefully, this work would stimulate further experiments to determine the nature of the states immediately above the Verwey transition and also the details of the charge-orbital ordering pattern in the low- T Cc structure.

ACKNOWLEDGMENTS

The authors gratefully acknowledge the support from the National Science Council of Taiwan. One of the authors (G.Y.G.) thanks Ying-Jer Kao for stimulating discussions on the entropy change at the Verwey transition.

*Electronic address: jeng@phys.sinica.edu.tw

†Electronic address: gyguo@phys.ntu.edu.tw

¹P. G. Radaelli, D. E. Cox, M. Marezio, and S. W. Cheong, *Phys. Rev. B* **55**, 3015 (1997).

²Y. Murakami, H. Kawada, H. Kawata, M. Tanaka, T. Arima, Y. Moritomo, and Y. Tokura, *Phys. Rev. Lett.* **80**, 1932 (1998).

³S. Mori, C. H. Chen, and S. W. Cheong, *Nature (London)* **392**, 473 (1998).

⁴S. B. Wilkins, P. D. Spencer, P. D. Hatton, S. P. Collins, M. D. Roper, D. Prabhakaran, and A. T. Boothroyd, *Phys. Rev. Lett.* **91**, 167205 (2003).

⁵J. M. Tranquada, B. J. Sternlieb, J. D. Axe, Y. Nakamura, and S. Uchida, *Nature (London)* **375**, 561 (1995).

⁶I. V. Solovyev and K. Terakura, *Phys. Rev. Lett.* **83**, 2825 (1999).

⁷J. van den Brink, G. Khaliullin, and D. Khomskii, *Phys. Rev. Lett.* **83**, 5118 (1999).

⁸P. Mahadevan, K. Terakura, and D. D. Sarma, *Phys. Rev. Lett.* **87**, 066404 (2001).

⁹Z. Popović and S. Satpathy, *Phys. Rev. Lett.* **88**, 197201 (2002).

¹⁰E. J. W. Verwey and P. Haayman, *Physica (Amsterdam)* **8**, 979 (1941); E. J. W. Verwey and E. L. Heilmann, *J. Chem. Phys.* **15**, 174 (1947); E. J. W. Verwey, P. W. Haayman, and F. C. Romeijn, *ibid.* **15**, 181 (1947).

¹¹See the review of research on the Verwey transition, J. García and G. Subías, *J. Phys.: Condens. Matter* **16**, R145 (2004); F. Walz, *ibid.* **14**, R285 (2002).

¹²P. W. Anderson, *Phys. Rev.* **102**, 1008 (1956).

¹³J. M. Zuo, J. C. H. Spence, and W. Petuskey, *Phys. Rev. B* **42**, 8451 (1990).

¹⁴F. J. Berry, S. Skinner, and M. F. Thomas, *J. Phys.: Condens. Matter* **10**, 215 (1998).

¹⁵P. Novák, H. Stepankova, J. Englich, J. Kohout, and V. A. M. Brabers, *Phys. Rev. B* **61**, 1256 (2000).

¹⁶J. P. Wright, J. P. Attfield, and P. G. Radaelli, *Phys. Rev. Lett.* **87**, 266401 (2001).

¹⁷J. P. Wright, J. P. Attfield, and P. G. Radaelli, *Phys. Rev. B* **66**, 214422 (2002).

¹⁸Z. Szotek, W. M. Temmerman, A. Svane, L. Petit, G. M. Stocks, and H. Winter, *Phys. Rev. B* **68**, 054415 (2003).

¹⁹H. T. Jeng, G. Y. Guo, and D. J. Huang, *Phys. Rev. Lett.* **93**, 156403 (2004).

²⁰I. Leonov, A. N. Yaresko, V. N. Antonov, M. A. Korotin, and V. I. Anisimov, *Phys. Rev. Lett.* **93**, 146404 (2004).

²¹G. Subías, J. García, J. Blasco, M. Grazia Proietti, H. Renevier, and M. Concepcion Sánchez, *Phys. Rev. Lett.* **93**, 156408 (2004).

²²G. K. Rozenberg, M. P. Pasternak, W. M. Xu, Y. Amiel, M. Hanfland, M. Amboage, R. D. Taylor, and R. Jeanloz, *Phys. Rev. Lett.* **96**, 045705 (2006).

²³D. J. Huang, H.-J. Lin, J. Okamoto, K. S. Chao, H.-T. Jeng, G. Y. Guo, C.-H. Hsu, C.-M. Huang, D. C. Ling, W. B. Wu, C. S. Yang, and C. T. Chen, *Phys. Rev. Lett.* **96**, 096401 (2006).

²⁴J. Schlappa, C. Schüßler-Langeheine, C. F. Chang, H. Ott, A. Tanaka, Z. Hu, M. W. Haverkort, F. Schierle, E. Weschke,

- G. Kaindl, and L. H. Tjeng, cond-mat/0605096 (to be published).
- ²⁵H. Uzu and A. Tanaka, J. Phys. Soc. Jpn. **75**, 043704 (2006).
- ²⁶E. J. Samuelsen and O. Steinsvoll, Phys. Status Solidi B **61**, 615 (1974).
- ²⁷M. Iizumi, T. F. Koetzle, G. Shirane, S. Chikazumi, M. Matsui, and S. Todo, Acta Crystallogr., Sect. B: Struct. Crystallogr. Cryst. Chem. **B38**, 2121 (1982).
- ²⁸J. García, G. Subías, M. G. Proietti, J. Blasco, H. Renevier, J. L. Hodeau, and Y. Joly, Phys. Rev. B **63**, 054110 (2001).
- ²⁹J. P. Shepherd, J. W. Koenitzer, R. Aragón, C. J. Sandberg, and J. M. Honig, Phys. Rev. B **31**, 1107 (1985).
- ³⁰J. P. Shepherd, J. W. Koenitzer, R. Aragón, J. Spátek, and J. M. Honig, Phys. Rev. B **43**, 8461 (1991); A. Kozłowski, Z. Kakol, D. Kim, R. Zalecki, and J. M. Honig, *ibid.* **54**, 12093 (1996).
- ³¹P. E. Blöchl, Phys. Rev. B **50**, 17953 (1994); G. Kresse and D. Joubert, *ibid.* **59**, 1758 (1999).
- ³²G. Kresse and J. Hafner, Phys. Rev. B **48**, 13115 (1993); G. Kresse and J. Furthmüller, Comput. Mater. Sci. **6**, 15 (1996); Phys. Rev. B **54**, 11169 (1996).
- ³³J. P. Perdew and Y. Wang, Phys. Rev. B **45**, 13244 (1992).
- ³⁴V. I. Anisimov, J. Zaanen, and O. K. Andersen, Phys. Rev. B **44**, 943 (1991).
- ³⁵A. I. Liechtenstein, V. I. Anisimov, and J. Zaanen, Phys. Rev. B **52**, R5467 (1995).
- ³⁶V. I. Anisimov, I. S. Elfimov, N. Hamada, and K. Terakura, Phys. Rev. B **54**, 4387 (1996).
- ³⁷See, e. g., H.-T. Jeng and G. Y. Guo, Phys. Rev. B **65**, 094429 (2002), and references therein.
- ³⁸S. K. Park, T. Ishikawa, and Y. Tokura, Phys. Rev. B **58**, 3717 (1998).
- ³⁹H. Seo, M. Ogata, and H. Fukuyama, Phys. Rev. B **65**, 085107 (2002).
- ⁴⁰S. M. Shapiro, M. Iizumi, and G. Shirane, Phys. Rev. B **14**, 200 (1976).
- ⁴¹J.-H. Park, L. H. Tjeng, J. W. Allen, P. Metcalf, and C. T. Chen, Phys. Rev. B **55**, 12813 (1997).